Bull. Chem. Soc. Ethiop. **2023**, 37(6), 1443-1457.
DOI: https://dx.doi.org/10.4314/bcse.v37i6.12

ISSN 1011-3924
Printed in Ethiopia
Online ISSN 1726-801X

EXPLORING NOVEL CORAL REEF-LIKE RuO_2 OXIDES: SYNTHESIS AND PHYSICOCHEMICAL CHARACTERIZATIONS OF GATIFLOXACIN-BASED Ru(III) COMPLEXES

Khaled Althubeiti*

Department of Chemistry, College of Science, Taif University, P.O. Box 11099, Taif 21944, Saudi Arabia

(Received June 2, 2023; Revised July 21, 2023; Accepted July 24, 2023)

ABSTRACT. Two mixed-ligand complexes of Ru(III) ions were synthesized and used to generate nanostructured RuO_2 oxide. Complex A contains gatifloxacin (L1), the amino acid glycine (L2), and Ru(III) ions in a 1:1:1 ratio. Complex B contains gatifloxacin (L1), the amino acid alanine (L3), and Ru(III) ions in a 1:1:1 ratio. The synthesized complexes were characterized using UV-Visible and IR spectroscopies, molar conductance, elemental analyses, thermogravimetry, XRD, and SEM-EDX techniques. In both complexes, the L1 ligand acts as a bidentate and uses the nitrogen atoms of the piperazine ring to capture the Ru(III) ions, while the L2 and L3 ligands capture the Ru(III) ions using their oxygen atom of the carboxylate group and the nitrogen atom of the amino group. The atmosphere around the Ru(III) ion is octahedral, and the complexes were formulated as $[RuL1L2(H_2O)_2]Cl_2$ and $[RuL1L3(H_2O)_2]Cl_2$ for Complex A and Complex B, respectively. Complex A was directly decomposed in air at 600 °C for 3 h to produce RuO_2 oxide (Oxide A), and complex B was decomposed under the same conditions to produce RuO_2 oxide (Oxide B). Morphologically, oxide A and oxide B have a coral reef-like texture with large holes and cavities.

KEY WORDS: Gatifloxacin, Ru(III) ion, Glycine, Alanine, Morphology, RuO_2 oxide

INTRODUCTION

The complexation of metal ions with biologically active molecules and drugs has garnered considerable interest from chemists and pharmacists alike. Many metallodrug and metal-based complexes are utilized to treat various human diseases due to their potential biological activities, such as anticancer, antibacterial, antifungal, and antiviral effects [1-3]. Metal-based complexes can be utilized in designing more biologically active drugs due to the ability of transition metals to interact with multiple metal-binding sites and the different oxidation states of transition metals, enabling the design of metallodrug complexes with more biological activities. Fluoroquinolones (FQs) are a class of compounds that possess strong and broad-spectrum antibacterial activities. They are extensively used due to their high potency, low price, and lack of cross-resistance. The interactions of metal ions with FQs antibiotics have attracted considerable attention as these interactions improve the biological and pharmaceutical properties of FQs antibiotics [4-6].

Gatifloxacin, a third-generation FQ antibiotic and exists as a white powder with a molecular weight of 375.4 g/mol, a linear molecular formula of $C_{19}H_{22}FN_3O_4$, a melting point of 220–225°C, and a chemical name of 1-cyclopropyl-6-fluoro-1,4-dihydro-8-methoxy-7-(3-methyl-1-piperazinyl)-4-oxo-3-quinoline carboxylic acid. It possesses strong antibacterial, antifungal, and anti-inflammatory properties [7]. The reaction of gatifloxacin with several metal ions, such as Co(II), Fe(III), Pt(II), Cd(II), Ni(II), Cr(III), Zn(II), and Pd(II) as a uni-dentate or bi-dentate ligand, has been investigated and discussed [8-13].

Several transition metal oxides, such as RuO_2, Co_3O_4, TiO_2, NiO, MnO_2, ZnO, In_2O_3, SnO_2, and TiO_2, are utilized as environmentally-friendly precursors for cleaning the environment by absorbing various toxic and hazardous substances, including pesticides, textile dyes, and

*Corresponding author. E-mail: k.Althubeiti@tu.edu.sa

discarded pharmaceutical drugs. These oxides possess strong photocatalytic properties and can be utilized to degrade such pollutants [14-17]. Preparing these transition metal oxides in the nanoscale range improves their reactive sites, increases their surface areas, and magnifies their ability to remove environmental pollutants [18]. RuO_2 oxide has several interesting properties, such as a wide potential window, rapid proton transfer, exceptional reversible redox transitions, mixed electro-protonic conductivity, and excellent specific capacitance [19].

The synthesis of new metallodrug complexes, especially those containing mixed ligands, may play a crucial role in developing effective metal-based drugs. This study investigated the synthesis, structural, thermal, and morphological characteristics of two mixed-ligand complexes containing Ru(III) ions and two ligands, gatifloxacin, and an amino acid. Additionally, the ability of these complexes to produce nanostructured RuO_2 oxide was examined. The study is divided into three sections:

(i) Complexes. Complex A was synthesized by reacting gatifloxacin and the amino acid glycine with Ru(III) ions in a MeOH:H_2O solvent mixture with a 1:1:1 (metal: antibiotic: amino acid) ratio at 80°C. Similarly, Complex B was synthesized using the same method and conditions but with alanine as the amino acid.

(ii) Oxides. To examine the ability of the synthesized complexes to provide nanostructured RuO_2 oxide, the complexes were decomposed in air at 600 °C for 3 h.

(iii) Chemical and physical characterizations. The synthesized complexes and the resulting oxides were characterized using various spectroscopic and physicochemical techniques, including UV-Visible and IR spectroscopies, CHN elemental analyses, conductivity measurements, thermogravimetry, XRD, and SEM-EDX.

EXPERIMENTAL

Chemicals and instruments

The ligands used in preparing the complexes were gatifloxacin ($C_{19}H_{22}FN_3O_4$; 375.4 g/mol; purity ≥ 98%) (referred to as L1), glycine amino acid (NH_2CH_2COOH; 75.07 g/mol; purity ≥ 99%) (referred to as L2), and L-alanine amino acid ($C_3H_7NO_2$; 89.09 g/mol; purity ≥ 98%) (referred to as L3). The L1 and L3 ligands were obtained from Fluka Company (Seelze, Germany), whereas the L2 ligand was provided by BDH Chemicals (UK). The ligands were complexed with Ru(III) ions: $RuCl_3 \cdot xH_2O$ (207.43 g/mol; anhydrous basis; purity 99.9%) obtained from the Sigma-Aldrich Company (St Louis, MO, USA). The methanol solvent was obtained from Merck KGaA company (Darmstadt, Germany) in analytical grade.

The FT-IR, UV-visible, and XRD spectra were collected at room temperature using a Shimadzu FT-IR spectrophotometer, a Perkin-Elmer Lambda 25 UV/Vis spectrophotometer, and an X'Pert Philips X-ray diffractometer, respectively. The FT-IR spectra were scanned in the range of 4000 to 400 cm^{-1}, the UV-visible spectra were scanned in the range of 300–1000 nm, and the XRD spectra were collected in the range of 2θ 20–100°. The contents of ruthenium metal and water were determined gravimetrically, while the contents of carbon, nitrogen, hydrogen, and chlorine in (%) were determined by a Perkin-Elmer 2400 series CHN elemental analyzer. The conductivity of the complexes was measured using a Jenway 4010 conductivity meter. The complexes were dissolved in dimethyl sulfoxide (DMSO) at a concentration of 1×10^{-3} M. Thermogravimetric analysis (TGA) and differential thermal analysis (DTA) thermograms were collected over the temperature range of 25–1000°C in a nitrogen atmosphere using a Shimadzu TG/DTG-50H thermal analyzer. The SEM-EDX data were collected using a Quanta FEI 250 scanning electron microscope (SEM) integrated with an EDAX detector. The instrument was operated at a 20 kV accelerating voltage.

Synthesis of complexes

Complex A was prepared by mixing 2 mmol of Ru(III) ions dissolved in 20 mL of deionized water, 2 mmol of L1 dissolved in 20 mL of methanol, and 2 mmol of L2 dissolved in 10 mL of deionized water. The pH of the resulting mixture was optimized at ~8 using drops of ammonium solution (5%). The resulting mixture was then refluxed for 6 h at 80 °C, gradually cooled, and left overnight at room temperature to yield dark-brown-colored precipitates. The dark-brown product obtained was separated, thoroughly washed with methanol, and dried under vacuum for 48 h. Complex B was synthesized similarly to Complex A, except that L3 was used instead of L2.

Synthesis of oxides

A simple method was used to decompose the synthesized complexes, which involved the calcination of Complex A and Complex B at 600 °C for 3 h in an electric furnace. The thermal decomposition product obtained was RuO_2 oxide, which was ground into a fine powder and characterized using FT-IR, XRD, and SEM-EDX data.

RESULTS AND DISCUSSION

Complexes A and B

Elemental and conductivity results

Complexes A and B were synthesized by reacting Ru(III) ions with two ligands at a pH of ~8 and a temperature of 80°C. The ligands in Complex A were L1 and L2, while the ligands in Complex B were L1 and L3. In both complexes, the reaction stoichiometry was 1:1:1 (Metal: antibiotic: amino acid), and the resulting products were dark-brown. The solubility tests indicated that complexes A and B were insoluble in water and most organic solvents, except DMSO and DMF. The contents of ruthenium metal and water in the complexes were determined gravimetrically, while the contents of carbon, nitrogen, hydrogen, and chlorine in (%) were determined by a CHN elemental analyzer. The elemental results of complexes A and B are listed in Table 1. The analytical data suggested that the general composition of Complex A is $[RuL1L2(H_2O)_2]Cl_2$ with a gross formula of $C_{21}H_{30}FN_4O_8RuCl_2$ (657.37 g/mol), whereas the general composition of Complex B is $[RuL1L3(H_2O)_2]Cl_2$ with a gross formula of $C_{22}H_{32}FN_4O_8RuCl_2$ (671.39 g/mol). These formulas suggest that complexes A and B possess an octahedral structure. Complexes A and B displayed high melting points of 270–275 °C for Complex A and 220–227 °C for Complex B. The molar conductance values of the free L1, L2, and L3 ligands were 0.15, 0.45, and 0.46 μS, respectively. After the Ru(III) ions were chelated by the ligands, the conductivity increased to 0.72 μS for Complex A and to 1.18 μS for Complex B. These values suggest that one or two chloride ions exist outside the complex's coordination sphere.

UV-visible spectral results

The UV-visible spectra of the free ligands, Complex A, and Complex B scanned over the 300–1000 nm wavelength range in DMSO solvent at room temperature. Three absorption bands were observed in the UV-visible spectrum of the free L1 ligand at 367, 354, and 339 nm. The bands located at 367 and 354 nm were assigned to the $n\rightarrow\pi^*$ transitions for the piperazine ring, carboxylic and ketonic groups. The $\pi\rightarrow\pi^*$ transitions of the aromatic ring in the L1 molecule were responsible for the absorption band at 339 nm. In complexes A and B, the characteristic absorption bands of the free L1 ligand were shifted to lower wavelengths due to intra-molecular interactions. These bands were observed at 360, 348, and 333 nm in the UV-visible spectrum of Complex A,

and at 352, 340, and 333 nm in the UV-visible spectrum of Complex B. The absorption band resonated at 348 nm (Complex A) and 340 nm (Complex B) could be assigned to the $_2T_{2g}\rightarrow{}_2A_{2g}$ transition, whereas the absorption band resonated at 333 nm (Complex A and Complex B) could be assigned to the $_2T_{2g}\rightarrow{}_4T_{1g}$ transition [20, 21].

Table 1. Physical data and elemental results for Complex A and Complex B.

Complex	Color	M.P. (°C)	Λm (μS)	Elemental results (%) calculated (found)				
				C	N	H	Ru	Cl
Complex A	Dark-brown	270-275	0.72	38.33 (38.56)	8.52 (8.37)	4.56 (4.45)	15.36 (15.54)	10.79 (10.58)
Complex B	Dark-brown	220-227	1.18	39.32 (39.05)	8.34 (8.50)	4.77 (4.90)	15.04 (14.88)	10.56 (10.74)

FT-IR spectral results

The FT-IR spectra of the free ligands, Complex A, and Complex B are illustrated in Figure 1. The free L1 molecule contains several different functional groups: C–F, C=C, C–O, C=O, O–H, C–N, and N–H. In addition to these functional groups, the L1 molecule possesses two $-CH_3$ and five $-CH_2$ groups. The functional groups displayed several absorption bands that appeared at 1146, 1207, 1546, 1622, 1721, 1318, 3223, and 3397 cm^{-1} originating from the ν(C–F), ν(C–O), ν(C=C), $\nu(C{=}O)_{ketonic}$, $\nu(C{=}O)_{carboxylic}$, $\nu_{sym}(C–N)$, ν(O–H), and $\nu(N–H)_{piperazine}$ vibrational modes, respectively. The bands resonated at 821 and 1438 cm^{-1} were generated from the $\delta_{wag}(CH_3)$ and $\delta_{rock}(CH_3)$ vibrations, respectively [22]. The bands located at 643, 730, 1268 and 1349 cm^{-1} originated from the $\delta_{twist}(CH_2)$, $\delta_{wag}(CH_2)$, $\delta_{rock}(CH_2)$, and $\delta_{sciss}(CH_2)$ vibrations, respectively [22]. The $\nu_{asym}(C–H)$ and $\nu_{sym}(C–H)$ vibrations of CH, CH_2, and CH_3 moieties were responsible for the absorption bands that appeared at 2844 and 2957 cm^{-1}.

Free L2 and L3 amino acids form the zwitterion structure in solution. In this structure, the amino group can accept a hydrogen ion and become positively charged or lose a hydrogen ion and become negatively charged. The IR data (cm^{-1}) of free L_2 molecule are: 900 $\delta_{rock}(CH_2)$, 1038 ν(C–N), 1110 $\delta_{rock}(NH_3)$, 1320 $\delta_{wag}(CH_2)$ and $\delta_{wag}(NH_3)$, 1400 $\nu_{sym}(COO)$, 1436 $\delta_{def}(CH_2)$, 1497 $\nu_{asym}(COO)$, 1585 $\delta(NH_3)$, 1740 $\nu(C{=}O)_{COOH}$, 2513 $\nu(CH_2)$, 2819, 2700 and 2603 $(–COOH\ldots NH_2–)_{hydrogen\ bond}$, and 3153 $\nu(NH_3)$ [23]. The IR data (cm^{-1}) of free L_3 molecule are: 641 $\delta_{twist}(CH_2)$, 769 $\delta_{wag}(CH_2)$, 843 $\delta_{wag}(CH_3)$, 917 $\delta_{rock}(CH_2)$, 1013 ν(C–N), 1110 $\delta_{rock}(NH_3)$, 1238 $\delta_{rock}(CH_2)$, 1302 $\delta_{wag}(CH_2)$, 1347 $\delta_{wag}(NH_3)$, 1411 $\nu_{sym}(COO)$, 1453 $\nu_{asym}(COO)$, 1581 $\delta(NH_3)$, 1736 $\nu(C{=}O)_{COOH}$, 2525 $\nu(CH_2)$, 2986, 2922 and 2864 [$\nu_{asym}(C–H)$ and $\nu_{sym}(C–H)$], 2800, 2731 and 2600 $(–COOH\ldots NH_2–)_{hydrogen\ bond}$, and 3075 $\nu(NH_3)$.

The IR spectrum of Complex A displayed absorption bands at 488, 647, 730, 797, 890, 938, 1000, 1045, 1098, 1130, 1272, 1314, 1398, 1442, 1511, 1616, 1728, 2483, (2805 and 2948), 3114, and 3380 cm^{-1} that originated, respectively, from the vibrations of [ν(Ru–O) and ν(Ru–N)], $\delta_{twist}(CH_2)$, $\delta_{wag}(CH_2)$, $\delta_{wag}(CH_3)$, $\delta_{def}(C–H)$, $\delta_{rock}(CH_2)$, δ(C–C), $\nu_{sym}(C–N)$, $\delta_{rock}(NH_2)$, ν(C–F), $\nu_{asym}(C–N)$, $\delta_{wag}(NH_2)$, $\nu_{sym}(COO)$, [$\delta_{def}(CH_2)$, $\delta_{sciss}(CH_2)$, and $\delta_{rock}(CH_3)$], $\nu_{asym}(COO)$, [$\nu(C{=}O)_{ketonic}$ and $\nu(C{=}O)_{carboxylic}$], $\nu(C{=}O)_{COOH}$, $\nu(CH_2)$, $\nu_{asym}(C–H)$ and $\nu_{sym}(C–H)$, [ν(O–H), and $\nu(NH_2)$], and $\nu(N–H)_{piperazine}$. The IR spectrum of Complex B generated absorption bands at 465, 647, 738, 887, 929, 995, 1049, 1098, 1129, 1268, 1325, 1405, 1435, 1509, 1606, 1725, 2480, (2804 and 2986), 3129, and 3365 cm^{-1} that originated, respectively, from the vibrations of [ν(Ru–O) and ν(Ru–N)], $\delta_{twist}(CH_2)$, $\delta_{wag}(CH_2)$, $\delta_{def}(C–H)$, $\delta_{rock}(CH_2)$, δ(C–C), $\nu_{sym}(C–N)$, $\delta_{rock}(NH_2)$, ν(C–F), $\nu_{asym}(C–N)$, $\delta_{wag}(NH_2)$, $\nu_{sym}(COO)$, [$\delta_{def}(CH_2)$, $\delta_{sciss}(CH_2)$, and $\delta_{rock}(CH_3)$], $\nu_{asym}(COO)$, [$\nu(C{=}O)_{ketonic}$ and $\nu(C{=}O)_{carboxylic}$], $\nu(C{=}O)_{COOH}$, $\nu(CH_2)$, $\nu_{asym}(C–H)$ and $\nu_{sym}(C–H)$ [ν(O–H), and $\nu(NH_2)$], and $\nu(N–H)_{piperazine}$.

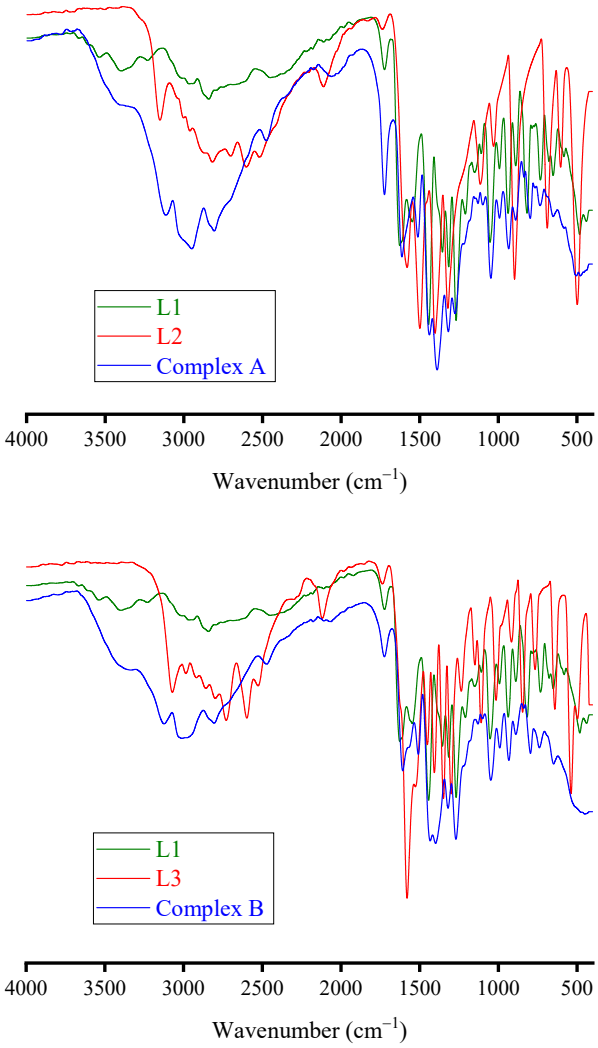

Figure 1. The IR spectra of the free ligands, Complex A, and Complex B.

The IR spectra of complexes A and B were characterized by a medium-intensity broad band in the range of 3200–2700 cm^{-1}. This broad band could result from the overlapping of ν_{asym}(C-H), ν_{sym}(C-H), ν(O-H), and ν(NH_2) vibrational modes. This band had three heads located at 2805, 2948, and 3114 cm^{-1} in Complex A and at 2804, 2986, and 3129 cm^{-1} in Complex B. The complexation of L1 with Ru(III) ions affected the intensity, broadening, and position of the band originating from the $\nu(N\text{-}H)_{piperazine}$ vibrations. In complexes, A and B, this band became broader, and its position was shifted to a lower wavenumber. The complexation process shifted several absorption bands resulting from the -CH_2 and -CH_3 vibrations. The complexation process also generated a new medium-intensity broad band in the range of 530 to 420 cm^{-1} in Complex A and

542 to 415 cm^{-1} in Complex B. This band could be attributed to the ν(Ru-N) and ν(Ru-O) vibrations [24]. Shifts were also observed in the vibrations resulting from the carboxylate group of L2 and L3 [ν_{asym}(COO) and ν_{sym}(COO)]. The values of the band shift, Δν [ν_{asym}COO - ν_{sym}COO], in Complex A and Complex B, suggested a unidentate coordination mode for the carboxylate group in L1 and L2, and the carboxylate group participated in the complexation process with Ru(III) ions [25]. All these observations proposed that the L1 ligand was coordinated to the Ru(III) ion via the nitrogen atoms of the piperazine ring, whereas the L2 and L3 ligands were coordinated to the Ru(III) ion via the carboxylate group's oxygen and the amino group's nitrogen atoms. All the ligands (L1, L2, and L3) act as bidentate ligands.

XRD spectral results

The XRD diffractograms of Complex A and Complex B are presented in Figure 2. Both complexes displayed similar XRD patterns. The absence of a strong and narrow sharp diffraction peak and the appearance of a broad peak ranging from 2θ ~ 25° to ~ 60° indicated that complexes A and B mainly have an amorphous structure. The broad peak contains a strong and sharp line at Bragg's angle 2θ 32.697° in Complex A and at 2θ 32.772° in Complex B. Complex A also had three low-intensity lines at Bragg's angle 2θ 46.812°, 52.811°, and 58.379°. Complex B also had three low-intensity lines located exactly at 2θ 46.842°, 52.912°, and 58.330°. The diffraction lines at (52.811°-52.912°), (46.812°-46.842°), and (32.697°-32.697°) are associated with Bragg's reflections (101), (100), and (002), respectively, for typical Ru metal [26]. The average particle diameters (*D*) for complexes A and B were calculated based on the intense Bragg's diffraction line detected in the complexes' XRD diffractograms using the Debye-Scherrer's law [D = 0.94 λ/β cos θ] [27]. The calculated *D* value was approximately 21.6 nm for Complex A and 21.8 nm for Complex B. These values suggest that complexes A and B are nanoscale-sized.

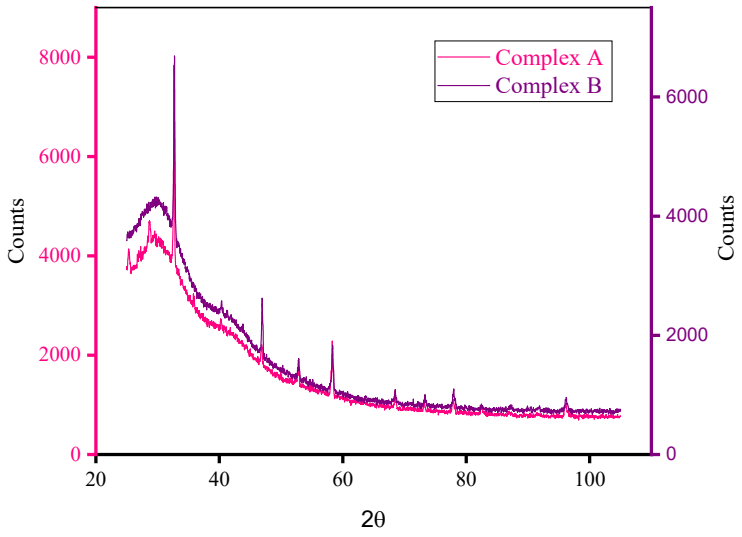

Figure 2. The XRD diffractograms of Complex A and Complex B.

Thermogravimetry

The thermograms of free L1 ligand, Complex A, and Complex B are scanned. Free L1 ligand was decomposed in three steps starting at 220°C and completed at 700°C, leaving no residual carbons. The first step from 220 °C to 315 °C corresponded to the loss of a cyclopropyl group and a methoxy group (18.95% weight loss). The second step, from 315 °C to 450 °C, corresponded to the loss of a 1-methyl piperazine moiety (26.55% weight loss). The last step occurred from 450 °C to 700 °C, corresponding to the loss of the 6-fluoro-1,4-dihydro-4-oxo-3-quinoline carboxylic acid organic moiety ($C_{10}H_3FNO_3$). Complex A exhibited a two-step decomposition pattern, starting at 50 °C and completing at 500 °C, with weight losses of 27.62% (observed) and 56.80% (observed) for the first and second steps, respectively. Two water molecules, Cl_2 and L2 ligand anion, were released in the first step. The pyrolysis of the L1 molecule began and was completed in the second degradation step, leaving Ru metal without any remaining carbons as the final decomposition product (15.29% weight loss). Complex B exhibited a three-step decomposition pattern, with weight losses of approximately 15.65%, 13.20%, and 55.77% for the first, second, and third steps, respectively. The first degradation step from 40°C to 160°C involved the removal of $2H_2O$ and Cl_2 molecules. The L3 ligand anion was released in the second step from 160 °C to 300 °C, followed by the release of the L1 ligand molecule in the final decomposition step from 300 °C to 445 °C. Complex B completely decomposed at ~550 °C, with Ru metal (15.21% weight loss) as the final thermal product. Strong endothermic peaks were observed in the DTA thermograms of both Complex A and Complex B in the 820–880°C and 800–900 °C ranges, respectively. These peaks, without any accompanying weight loss, could be attributed to the formation of nanostructured Ru metal with altered physicochemical transformation states [21, 28].

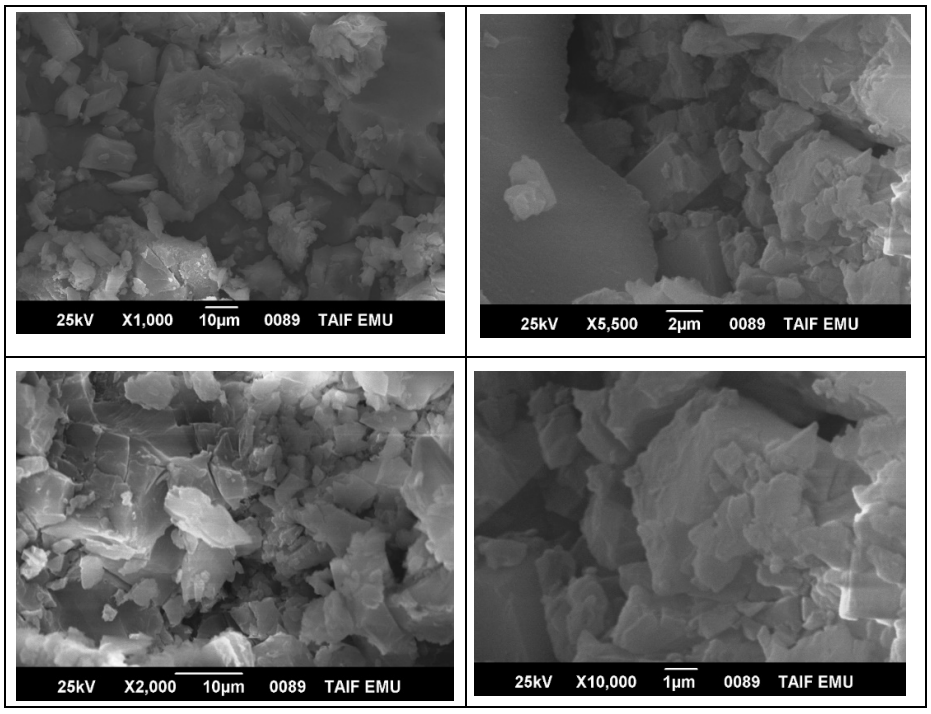

Figure 3. The SEM micrographs of Complex A.

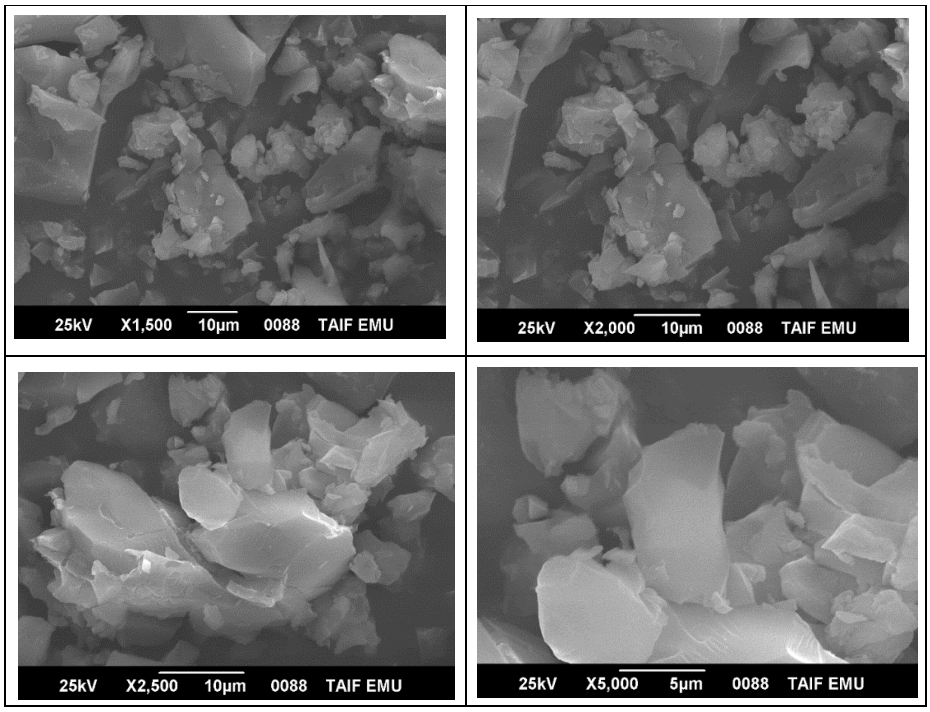

Figure 4. The SEM micrographs of Complex B.

SEM micrographs

A Quanta FEI 250 SEM instrument was used to visualize the SEM micrographs of Complexes A and B. The obtained micrographs are shown in Figures 3 and 4. These micrographs, captured at different magnification levels, provide information related to the outer surface (such as surface topology, porous structure, shape, and size of particles). The SEM micrographs captured between 1000× to 10,000× magnification reveal no differences in the shape and surface topology of the microstructure between Complex A and Complex B. Both complexes comprise large aggregates with irregular shapes, sizes, and features. SEM micrographs taken at high magnifications (5,000×) indicate that most of the aggregate surfaces are smooth and free from gaps or cracks. Some of the aggregates were broken into smaller pieces, which were differently sized and shaped.

Proposed structures

Based on the elemental, thermal, and spectral data, all three ligands (L1, L2, and L3) appear to act as bidentate ligands. L1 ligand was coordinated to the Ru(III) ions via the nitrogen atoms of the piperazine ring (NN coordination sites), while L2 and L3 ligands were coordinated to the Ru(III) ions via the oxygen atom of the carboxylate group and the nitrogen atom of the amino group (NO coordination sites). The atmosphere around the Ru(III) ion is octahedral, and the complexes were formulated as $[RuL1L2(H_2O)_2]Cl_2$ and $[RuL1L3(H_2O)_2]Cl_2$ for Complex A and Complex B, respectively. Two water molecules completed the coordination sphere of the six-coordinate mode of the Ru(III) ion (Figure 5).

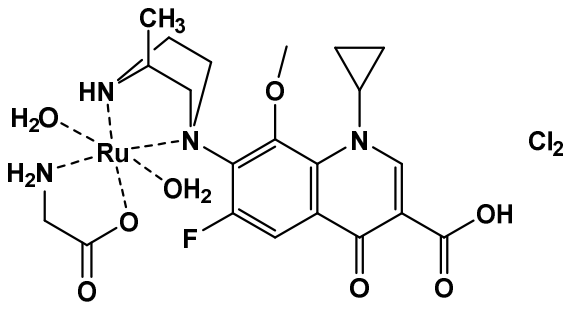

Complex A

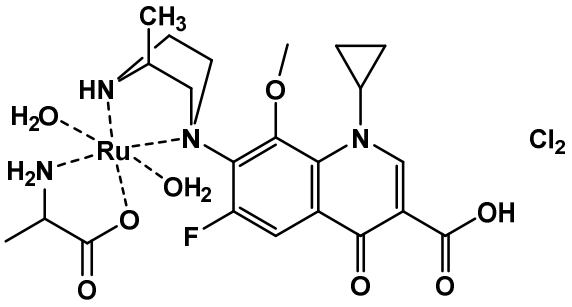

Complex B

Figure 5. Proposed chemical structure of complexes A and B.

Oxides A and B

SEM-EDX data

The direct thermal decomposition of complexes A and B in an electric furnace at 600 °C for 3 h produced the metal oxide RuO_2. The oxide obtained from Complex A was termed Oxide A, while the oxide obtained from Complex B was termed Oxide B. The EDX profiles of Oxides A and B (Figure 6) indicate that the obtained oxides are highly pure, containing only ruthenium and oxygen elements. The EDX spectrum for Oxide A displayed a strong, intense peak at 2.558 keV (ruthenium, mass 75.51%) and a weak peak at 0.525 keV (oxygen, mass 24.49%). The EDX spectrum for Oxide B displayed a strong, intense peak at 2.558 keV (ruthenium, mass 75.70%) and a weak peak at 0.525 keV (oxygen, mass 24.30%). The masses (%) obtained by EDX analysis for ruthenium and oxygen elements are in total agreement with the corresponding theoretical values (Ru 75.94% and O 24.06%) calculated from the chemical formula of RuO_2.

The microstructures of Oxides A and B were visualized using an SEM instrument, and the resulting micrographs are shown in Figures 7 and 8. SEM micrographs captured between 500× to 10,000× magnification indicate that Oxides A and B have an interesting morphology. These micrographs show that the oxides have a coral reef-like texture with large holes and cavities.

These holes and cavities are clearly visible in low magnification micrographs (500× and 1000×) as well as in high magnification micrographs (5,000× and 10,000×). The magnified micrographs show that the cavities have thick walls. The holes and cavities offer the oxides a large surface area and high absorption capacity, making them useful as catalysts for the heterogeneous degradation of organic pollutants (such as pesticides, textile dyes, and discarded pharmaceutical drugs).

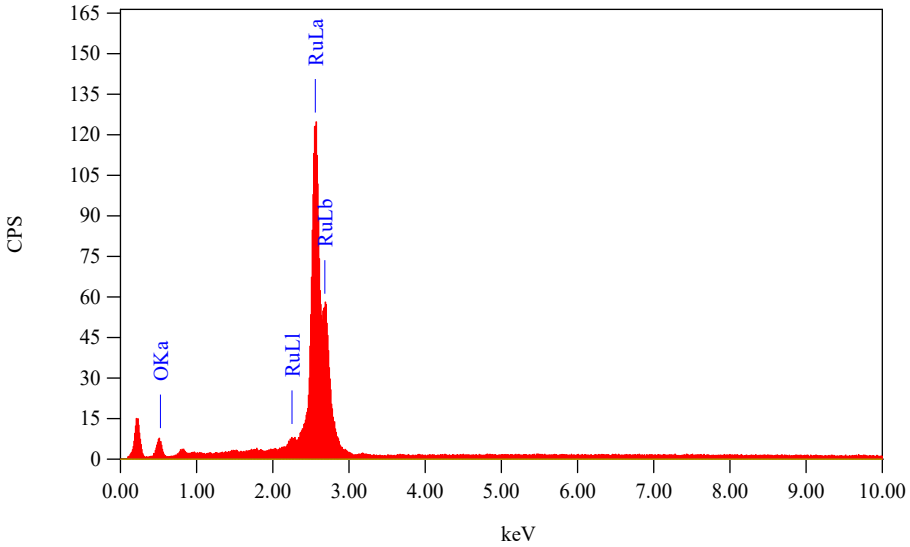

Figure 6a. The EDX spectrum of Oxide A.

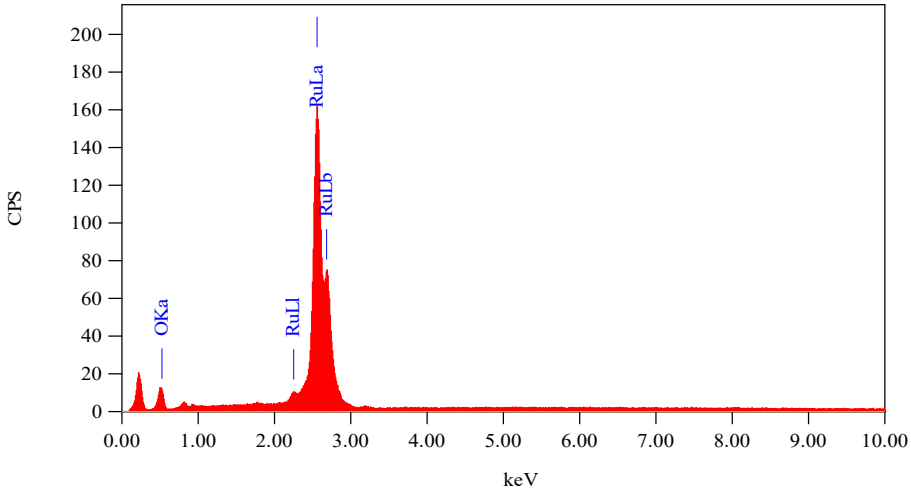

Figure 6b. The EDX spectrum of Oxide B.

FT-IR and XRD spectral results

The FT-IR and XRD spectra of the manufactured oxides are investigated. Both oxides displayed three absorption bands in the region 1200–1700 cm^{-1}. These bands are a strong absorption band resonating at 1740 cm^{-1} in the IR spectrum of Oxide A and at 1730 cm^{-1} in the IR spectrum of Oxide B, and two medium-intensity bands at 1371 and 1218 cm^{-1} for Oxide A and at 1364 and 1220 cm^{-1} for Oxide B. These bands could be attributed to the vibrations of physically adsorbed water (moisture) on the oxide's surface. The absorptions at 1218–1220 cm^{-1}, 1371–1365 cm^{-1}, and 1740–1730 cm^{-1} were assigned to the vibrations of peroxo groups (ν4), peroxo groups (ν5), and ν(O–H) of molecular water (ν6), respectively. A weak absorption band appeared at around ~530 in the IR spectra of both oxides and could be attributed to the (ν1) asymmetric stretching vibration characteristic of RuO_2 [29, 30].

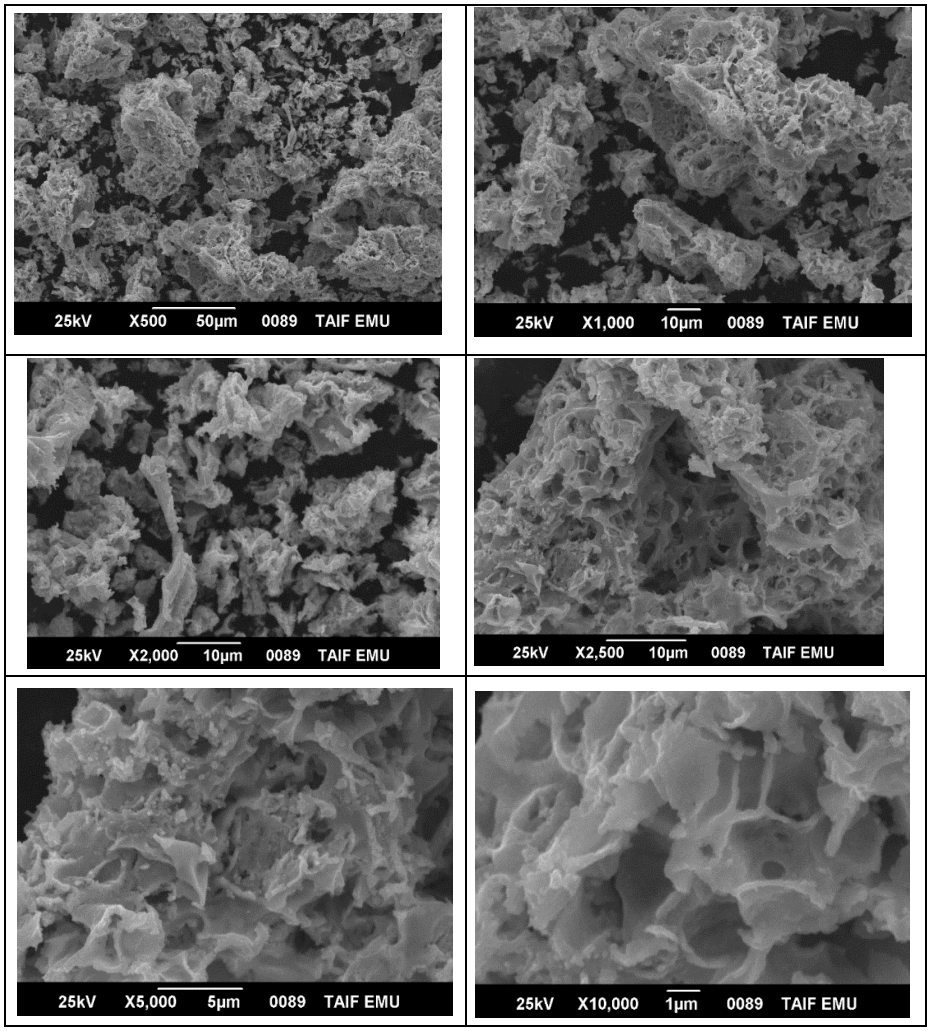

Figure 7. The SEM micrographs of Oxide A.

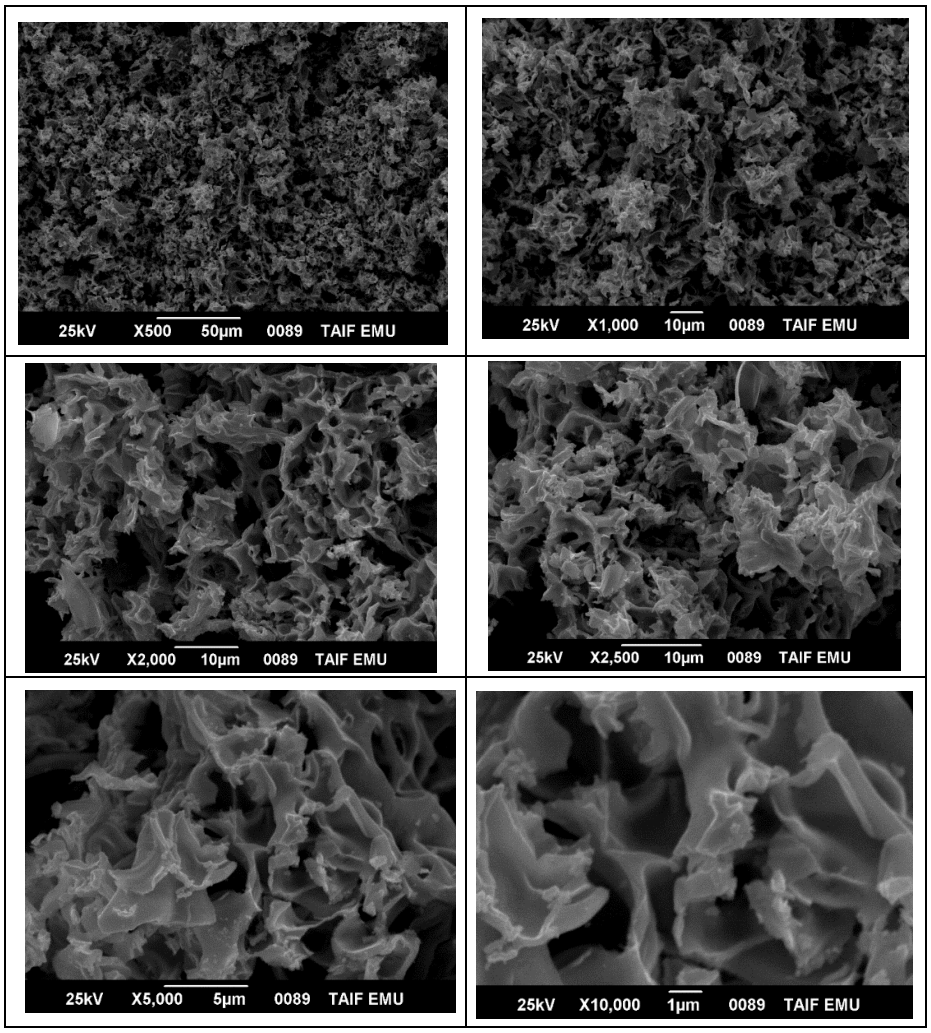

Figure 8. The SEM micrographs of Oxide B.

The XRD diffractograms of Oxide A and Oxide B are presented in Figure 9. The diffractograms indicate that both complexes display similar XRD patterns. A strong and narrow sharp diffraction line is observed at Bragg's angle 2θ 44.033° in the XRD spectrum of Oxide A and at Bragg's angle 2θ 44.133° in the XRD spectrum of Oxide B. Oxide A also has eight medium-intensity lines located exactly at 2θ values of 28.057°, 35.105°, 54.241°, 58.0°, 69.289°, 78.117°, 84.612°, and 85.891°. These lines appear at 2θ values of 28.158°, 35.130°, 54.240°, 58.228°, 69.439°, 78.418°, 84.587°, and 85.866° in the XRD spectrum of Oxide B. The diffraction lines at (28.105°-28.105°), (42.059°-42.059°), (44.070°-44.070°), (54.330°-54.330°), (69.473°-69.473°), and (78.358°-78.358°) can be assigned to the (311), (301), (220), (210), (020), and (110) reflections of the crystal RuO_2 phase, respectively [26]. The obtained reflections suggest that Oxide A and Oxide B have an orthorhombic structure (JCPDS No: 88−0323), which is in

agreement with those previously reported by Refat *et al.* [31] and Alibrahim *et al.* [32]. The *D* value for oxides A and B was calculated based on the intense Bragg's diffraction line detected in the oxides' XRD diffractograms using Debye-Scherrer's law [27]. The calculated *D* value was approximately 27.80 nm for Oxide A and approximately 29.25 nm for Oxide B. These values suggest that the crystallites of Oxides A and B are in the nanoscale range.

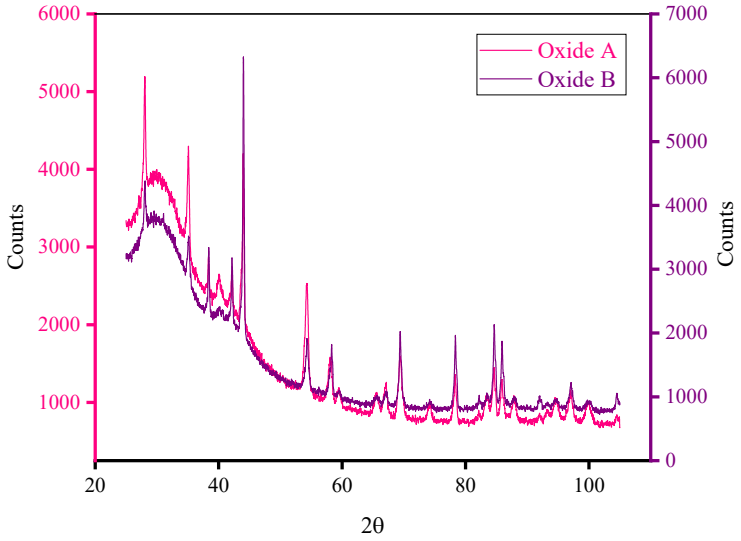

Figure 9. The XRD diffractograms of Oxide A, and Oxide B.

CONCLUSIONS

This study aimed to (1) present the synthesis of two mixed-ligand complexes of Ru(III) ions, Complex A and Complex B. Complex A contains the drug gatifloxacin (L1), the amino acid glycine (L2), and Ru(III) ions, whereas Complex B contains L1, the amino acid alanine (L3), and Ru(III) ions. (2) Decompose the synthesized complexes to generate the RuO_2 oxide. (3) Evaluate the molecular structure of the synthesized complexes using elemental, spectral, and thermal data. (4) Observe the X-ray structures, phase purity, and surface morphologies of the manufactured oxides. We found that the L1 ligand acts as a bidentate and captures the Ru(III) ions using the nitrogen atoms of the piperazine ring, while L2 and L3 ligands capture the Ru(III) ions using the oxygen atom of the carboxylate group and the nitrogen atom of the amino group. The complexes were formulated as $[RuL1L2(H_2O)_2]Cl_2$ and $[RuL1L3(H_2O)_2]Cl_2$ for Complex A and Complex B, respectively. Burning Complex A and Complex B at 600 °C for 3 h resulted in the formation of highly homogenized and uniform RuO_2 oxides with coral reef-like shaped morphology. The coral reef-like textures of the manufactured oxides have large holes and cavities, which offer the oxides a large surface area and high absorption capacity. The interesting surface topology of the manufactured oxides encourages future investigations into their potential as catalysts for the heterogeneous degradation of various organic pollutants.

ACKNOWLEDGEMENT

The researchers would like to acknowledge Deanship of Scientific Research, Taif University for funding this work.

REFERENCES

1. Tella, A.C.; Obaleye, J.A.; Olawale, M.D.; Ngororabanga, J.M.V.; Ogunlaja, A.S.; Bourned, S.A. Synthesis, crystal structure, and density functional theory study of a zinc(II) complex containing terpyridine and pyridine-2,6-dicarboxylic acid ligands: Analysis of the interactions with amoxicillin. *C.R. Chimie* **2019**, 22, 3-12.
2. El-Sonbati, A.Z.; Diab, M.A.; El-Bindary, A.A.; Abou-Dobara, M.I.; Seyam, H.A. Molecular docking, DNA binding, thermal studies and antimicrobial activities of Schiff base complexes. *J. Mol. Liq*. **2016**, 218, 434-456.
3. Ghoneim, M.M.; El-Sonbati, A.Z.; El-Bindary, A.A.; Diab, M.A.; Serag, L.S. Polymer complexes. LX. Supramolecular coordination and structures of N(4-(acrylamido)-2-hydroxybenzoic acid) polymer complexes, *Spectrochim. Acta Part A* **2015**, 140, 111-131.
4. Aljohani, M. Preparation and chemical study on metallic bonding with antibiotics in nanometer form to raise the therapeutic efficiency: structural characterizations of Cu(II), Co(II) and Ni(II) 6-aminopenicillinic acid complexes. *Bull. Chem. Soc. Ethiop*. **2023**, 37, 91-100.
5. Shaikh, Z.; Ashiq, U.; Jamal, R.A.; Gul, S.; Mahroof-Tahir, M.; Sultan, S.; Salar, U.; Khan, K.M. Synthesis, characterization, lipoxygenase, and tyrosinase inhibitory activities of non-cytotoxic titanium(III) and (IV) hydrazide complexes. *Bull. Chem. Soc. Ethiop*. **2023**, 37, 315-333.
6. Adam, A.M.A.; Refat, M.S.; Gaber, A.; Grabchev, I. Complexation of alkaline earth metals Mg2+, Ca2+, Sr2+ and Ba2+ with adrenaline hormone: Synthesis, spectroscopic and antimicrobial analysis. *Bull. Chem. Soc. Ethiop*. **2023**, 37, 357-372.
7. Oliphant, C.M.; Green, G.M. Quinolones: A comprehensive review. *Am. Fam. Phys*. **2002**, 65, 455-464.
8. Mehrotra, R.; Shukla, S.N.; Gaur, P.; Dubey, A. Identification of pharmacophore in bioactive metal complexes: Synthesis, spectroscopic characterization and application. *Eur. J. Med. Chem*. **2012**, 50, 149-153.
9. Vieira, L.M.M.; de Almeida, M.V.; Lourenço, M.C.S.; Bezerra, F.A.F.M.; Fontes, A.P.S. Synthesis and antitubercular activity of palladium and platinum complexes with fluoroquinolones. *Eur. J. Med. Chem*. **2009**, 44, 4107-4111.
10. Patel, M.N.; Gandhi, D.S.; Parmar, P.A. DNA interaction and in-vitro antibacterial studies of fluoroquinolone based platinum(II) complexes. *Inorg. Chem. Commun*. **2012**, 15, 248-251.
11. Li, Z.-Q.; Wu, F.-J.; Gong, Y.; Hu, C.-W.; Zhang, Y.-H.; Gan, M.-Y. Synthesis, characterization and activity against staphylococcus of metal(II)-gatifloxacin complexes. *Chin. J. Chem*. **2007**, 25, 1809-1814.
12. Sultana, N.; Naz, A.; Arayne, M.S.; Ahmed, M.M. Synthesis, characterization, antibacterial, antifungal and immunomodulating activities of gatifloxacin–metal complexes. *J. Mol. Struct*. **2010**, 969, 17-24.
13. Shaikh, A.R.; Giridhar, R.; Megraud, F.; Yadav, M.R. Metalloantibiotics: Synthesis, characterization and antimicrobial evaluation of bismuth-fluoroquinolone complexes against Helicobacter pylori. *Acta Pharm*. **2009**, 59, 259-271.
14. Al-Hazmi, G.H.; Adam, A.M.A.; El-Desouky, M.G.; El-Bindary, A.A.; Alsuhaibani, A.M.; Refat, M.S. Efficient adsorption of Rhodamine B using a composite of Fe_3O_4@zif-8: Synthesis, characterization, modeling analysis, statistical physics and mechanism of interaction. *Bull. Chem. Soc. Ethiop*. **2023**, 37, 211-229.
15. Williams, I.B.I.; Fodjo, E.K.; Narcisse, P.B.B.; Martin, A.A.; Sylvestre, K.K.K.; Albert, T.; Gu, Z. Effect of synthesized carbon quantum dots on the photocatalytic properties of ZnO. *Bull. Chem. Soc. Ethiop*. **2023**, 37, 463-476.
16. Allasi, H.L.; Rajalingam, A.A.; Jani, S.P.; Uppalapati, S. Influence of synthesized (green) cerium oxide nanoparticle with neem (*Azadirachta indica*) oil biofuel. *Bull. Chem. Soc. Ethiop*. **2023**, 37, 477-490.

17. Waheed, Z.; Ghazanfar, S.; Usman, M.; Asif, H.M.; Tariq, M.; Mahmood, K.; Haider, A.; Sirajuddin, M. Synthesis and characterization of ternary composite g-C_3N_4-WO_3/rGO for photocatalytic activity in degradation of methylene blue. *Bull. Chem. Soc. Ethiop*. **2023**, 37, 1123-1131.
18. Nagaraja, R.; Nagappa, B.; Girija, C.R.; Nagabhushana, B.M. Synthesis and characterization of nanocrystalline MgO powder and its application in the treatment of pharmaceutical effluent. *J. Nanotech. Appl*. 2011, 11, 28-32.
19. Fugare, B.Y.; Lokhande, B.J. Study on structural, morphological, electrochemical and corrosion properties of mesoporous RuO2 thin films prepared by ultrasonic spray pyrolysis for supercapacitor electrode application. *Mater. Sci. Semicond. Process* **2017**, 71, 121-127.
20. Althubeiti, K. In binary solvent: Synthesis and physicochemical studies on the nano-metric palladium(II) oxide associated from complexity of palladium(II) ions with gatifloxacin drug as a bio-precursors. *J. Mol. Struct*. **2020**, 1205, 127604.
21. Naglah, A.M.; Al-Omar, M.A.; Almehizia, A.A.; Obaidullah, A.J.; Bhat, M.A.; Al-Shakliah, N.S.; Belgacem, K.; Majrashi, B.M.; Refat, M.S.; Adam, A.M.A. Synthesis, spectroscopic, and antimicrobial study of binary and ternary ruthenium(III) complexes of ofloxacin drug and amino acids as secondary ligands. *Crystals* **2020**, 10, 225.
22. Sathyanarayana, D.N. *Vibrational Spectroscopy - Theory and Applications*, 2nd ed., New Age International (P) Limited Publishers: New Delhi; **2004**.
23. Maté, B.; Rodriguez-Lazcano, Y.; Gálvez, Ó.; Tanarroa, I.; Escribano, R. An infrared study of solid glycine in environments of astrophysical relevance. *Phys. Chem. Chem. Phys*. **2011**, 13, 12268-12276.
24. Nakamoto, K. *Infrared Spectra of Inorganic and Coordination Compounds*, 2nd ed., Wiley Interscience: New York; **1970**.
25. Deacon, G.B.; Phillips, R. Relationships between the carbon-oxygen stretching frequencies of carboxylato complexes and the type of carboxylate coordination. *Coord. Chem. Rev*. **1980**, 33, 227-250.
26. Singh, J.P.; Karabacak, T.; Morrow, P.; Pimanpang, S.; Lu, T.-M.; Wang, G.-C. Preferred orientation in Ru nanocolumns induced by residual oxygen. *J. Nanosci. Nanotechnol.* **2007**, 7, 2192-2196.
27. Estermann, M.A.; David, W.I.F. in: David, W.I.F.; Shankland, K.; Mccusker, I.B. Ch. Baerlocher (Eds.), *Structure Determination from Powder Diffraction Data (SDPD)*, Oxford Science Publications: New York; **2002**.
28. Alghamdi, M.T.; Alsibaai, A.A.; Shahawi, M.S.; Refat, M.S. Synthesis and spectroscopic studies of levofloxacin uni-dentate complexes of Ru(II), Pt(IV) and Ir(III): Third generation of quinolone antibiotic drug complexes. *J. Mol. Liq*. **2016**, 224, 571-579.
29. Chen, L.; Yuan, C.; Gao, B.; Chen, S.; Zhang, X. Microwave-assisted synthesis of organic–inorganic poly(3,4-ethylenedioxythiophene)/$RuO_2{\cdot}xH_2O$ nanocomposite for supercapacitor. *J. Solid-State Electrochem*. **2009**, 13, 1925-1933.
30. Sugimoto, W.; Iwata, H.; Murakami, Y.; Takasu, Y. Electrochemical capacitor behavior of layered ruthenic acid hydrate. *J. Electrochem. Soc*. **2004**, 151, A1181-A1187.
31. Refat, M.S.; Saad, H.A.; Gobouri, A.A.; Alsawat, M.; Belgacem, K.; Majrashi, B.M.; Adam, A.M.A. RuO_2 nanostructures from Ru(III) complexes as a new smart nanomaterials for using in the recycling and sustainable wastewater treatment: Synthesis, characterization, and catalytic activity in the hydrogen peroxide decomposition. *Russ. J. Phys. Chem. A* **2021**, 95, S346–S351.
32. Alibrahim, K.A.; Al-Fawzan, F.F.; Refat, M.S. Chemical preparation of nanostructures of Ni(II), Pd(II), and Ru(III) oxides by thermal decomposition of new metallic 4-aminoantipyrine derivatives. catalytic activity of the oxides. *Russ. J. Gen. Chem.* **2019**, 89, 2528-2533.